Wind and Structures, *Vol. 21, No. 4 (2015) 383-405*
DOI: http://dx.doi.org/10.12989/was.2015.21.4.383

Pressure measurements on inclined square prisms

Gang Hu[*1,2], K.T. Tse[1a], K.C.S. Kwok[1,2b] and Z.S. Chen[1c]

[1]*Department of Civil and Environmental Engineering, The Hong Kong University of Science and Technology, Clear Water Bay, Kowloon, Hong Kong, China*
[2]*Institute for Infrastructure Engineering, Western Sydney University, Penrith, NSW, 2751, Australia*

(Received June 7, 2015, Revised July 20, 2015, Accepted September 21, 2015)

Abstract. This study investigated aerodynamic characteristics of an inclined square prism experimentally. Pressure measurements were performed on a static square prism with a series of inclinations including forward inclinations (inclined to the upwind direction) and backward inclinations (inclined to the downwind direction). The prism with a vertical attitude was also tested for comparisons. Based on the pressure data, influences of the inclinations on aerodynamic characteristics (e.g., force coefficients, pressure distributions on the surfaces, and vortex shedding features) of the square prism were evaluated in detail. The results show that the inclinations have significant effects on these aerodynamic characteristics. Furthermore, the influences of the forward and backward inclinations are quite different.

Keywords: aerodynamic characteristic; inclined prism; wind tunnel test; square prism

1. Introduction

Aerodynamic characteristics of a finite square prism are a topic of great practical importance. Tall buildings, bridge towers, and landmarks are some of the examples. Their aerodynamic characteristics determine their flow-induced behaviors, which are associated with structure safety. Therefore, aerodynamic characteristics of this type of structure have been widely studied. For instance, Kwok and Melbourne (1981) investigated wind-induced lock-in excitation of tall structures experimentally. Kareem and Cermak (1984) and Kareem (1990) investigated pressure features on the surfaces of square building models. Lin *et al.* (2005) assessed characteristics of wind forces on tall buildings with different rectangular cross-sections in detail. Tanaka *et al.* (2012) evaluated aerodynamic forces and pressures acting on tall building models with unconventional configurations.

The majority of previous studies were devoted to study aerodynamic characteristics of square prisms with their principal axes perpendicular to the oncoming flow, e.g., tall buildings subject to a boundary layer flow. However, some slender structures in reality, such as the pylon of the Alamillo Bridge in Spain, are inclined. Hu *et al.* (2015b) have investigated galloping behaviors of an

*Corresponding author, Research Associate, E-mail: ghuaaust@gmail.com
[a] Assistant Professor, E-mail: timkttse@ust.hk
[b] Emeritus Professor, E-mail: K.Kwok@uws.edu.au
[c] Ph.D. Student

http://www.techno-press.org/?journal=was&subpage=8 ISSN: 1226-6116 (Print), 1598-6225 (Online)

inclined square prism. Their study shows that the inclinations have significant effects on the galloping behaviors. Therefore, it is anticipated that the inclination of the slender structure has a non-negligible impact on the aerodynamic characteristics.

The study described here aims to investigate effects of inclinations on aerodynamic characteristics of a square prism by measuring pressures acting on the surfaces in a wind tunnel. The pressure tests were performed on a static square prism with different inclinations, including forward inclinations (inclined to the upwind direction), a vertical attitude, and backward inclinations (inclined to the downwind direction). Force coefficients, pressure distributions on the surface, spectra and coherences of pressures, and Strouhal numbers of inclined prisms were analyzed.

2. Experimental setup of pressure tests

Pressure measurements were carried out in the high-speed test section (3×2 m^2) of the CLP Power Wind/Wave Tunnel Facility at the Hong Kong University of Science and Technology. Tests were performed under a turbulent flow in the upstream fetch of the test section. Comparisons between the measured profiles and the target profiles, corresponding to the open terrain (i.e., Category 2) in the AS/NZS 1170.2:2002 (Standards Australia/Standards New Zealand 2002), show good agreements as shown in Fig. 1. The mean wind speed was normalized by the corresponding value at the vertical prism top. The normalized spectrum of longitudinal velocity component at the vertical prism top is given in Fig. 2.

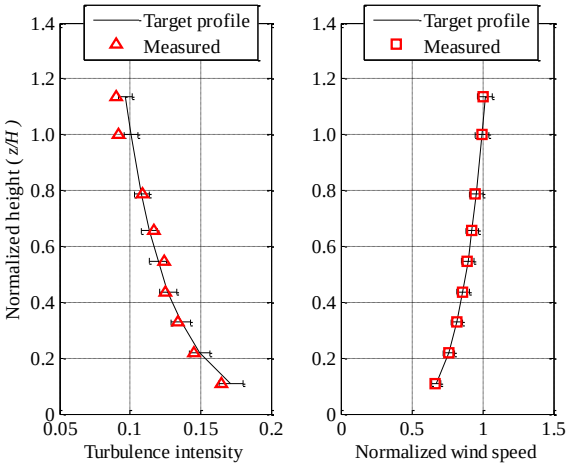

Fig. 1 Turbulent wind flow field adopted in pressure tests

Table 1 Inclination angles of the prism for wind tunnel tests

α (°)	0	±5	±10	±15	±20	±25	±30	±35

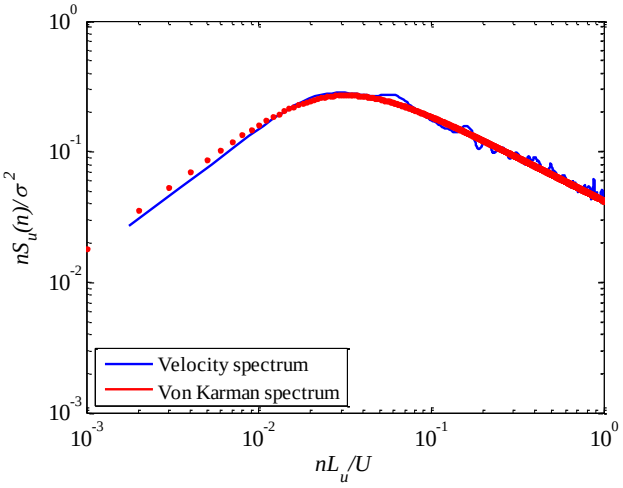

Fig. 2 Normalized spectrum of longitudinal velocity

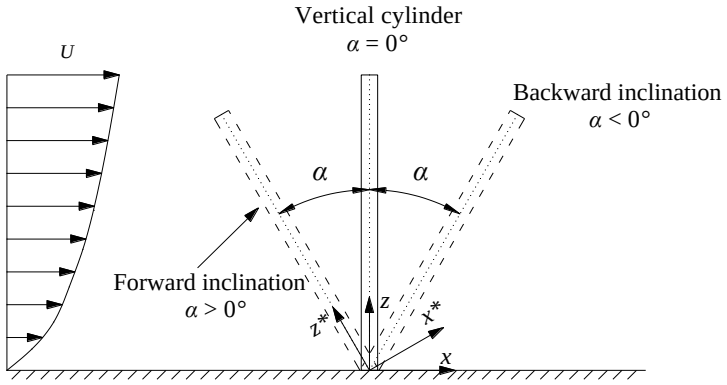

Fig. 3 Tested three different types of prisms: forward inclined prism, vertical prism, and backward inclined prism. α is angle of inclination: a positive value represents forward inclination while a negative one denotes backward inclination

The model was made by a square aluminum hollow prism with width D = 5.08 cm (2 inches) and height H = 91.44 cm (36 inches). The blockage ratio of the model in the wind tunnel was about 0.8%, which is much lower than the critical value of 5% (Holmes 2015). The inclination angle α of the prism took the values listed in Table 1 whilst the definitions of inclinations are given in Fig. 3. Pressures acting on the surfaces of the rigid model were collected through a synchronous multi-pressure sensing system (SMPSS), and the total number of pressure taps was 220. The 220 pressure taps were distributed among 11 levels over the span, 20 taps on each level, and 5 taps for each side on each level. Pressure taps on one side face is shown in Fig. 4; the tap distribution on the other faces is the same. The measurements were taken by using high-speed scanning pressure equipment and 14 electronic pressure scanners. The sampling frequency and duration were set to 400 Hz and 120 seconds respectively. The reference point was taken at the top of the vertical prism,

and the corresponding mean velocity, i.e., V_{ref}, was kept at a constant of approximately 12 m/s regardless of the inclination. The Reynolds number *Re* based on the width *D* and the reference velocity V_{ref}, was 4×10^4. All the tests were performed at a zero wind incidence angle. More details of the experiment can be found in Hu *et al.* (2015b).

3. Results and discussions

3.1 Mean pressure distribution on the prism face

Mean pressure coefficients on the windward face of the prism with different inclinations are presented in Fig. 5. It is well known that there is a stagnation region on the windward face of a vertical prism at a height of 70% to 80% (Holmes 2015). The stagnation region corresponds to the maximum mean pressure location where the approaching flow splits into an upwash, a downwash and horizontal flow. In the present study, for the vertical case (i.e., α = 0°) the stagnation pressure coefficient is 0.9, which appears near the free end reasonably. With increasing the forward inclination, the stagnation region moves upward. Meanwhile, both the stagnation pressure coefficient and the pressure coefficients on the overall face substantially decrease. Similarly, the pressure coefficients decrease with increasing the backward inclination as well. However, contrary to the forward inclination, the backward inclination moves the stagnation region downward. Based on the effects of the forward and backward inclinations on the location of the stagnation region, it is interesting to note that as the free end of the prism is inclined from upstream to downstream (i.e., from α = 35° to 0° and then to -35°), the stagnation region gradually moves downward. That is to say, the stagnation region moves toward the upstream end of the inclined prism.

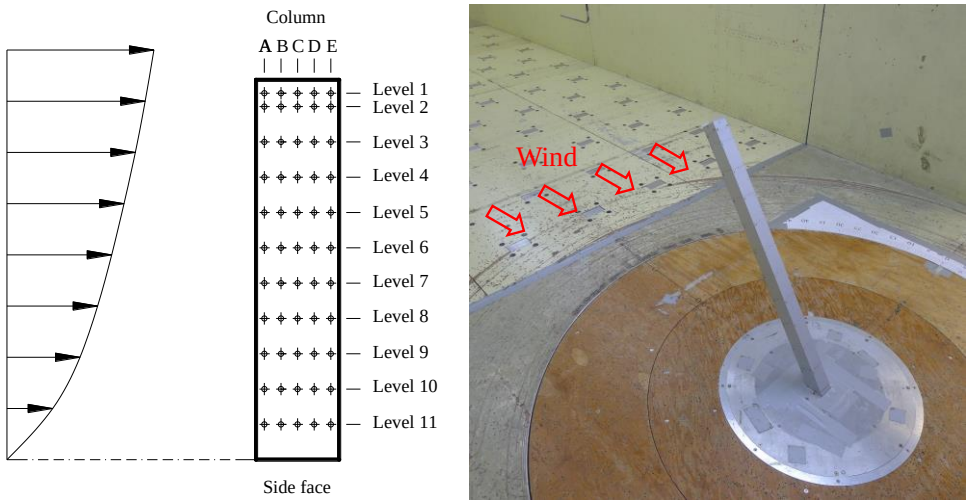

Fig. 4 Model for pressure measurements: (a) distribution and label of pressure taps on side face, (b) square-section prism with a forward inclination angle in wind tunnel

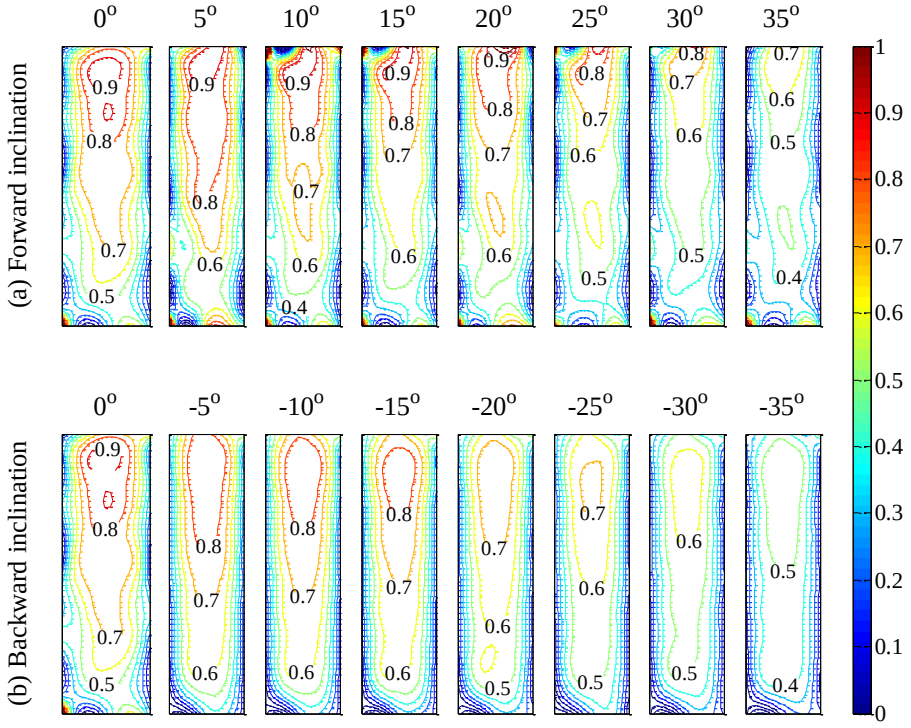

Fig. 5 Mean pressure coefficients on the windward face with different inclinations

Mean pressure coefficients on the side face of the prism with different inclinations are shown in Fig. 6. Apart from the region near the free end, the pressure coefficient generally increases with increasing the forward inclination on the overall face as shown in Fig. 6(a). The increases can be attributed to a decrease in the curvature of the separated shear layer in the corresponding height as suggested by Hu *et al.* (2015a). The pressure distribution in the region near the free end is more complicated. In detail, at the upstream corner of the free end of the vertical prism (i.e., α = 0°), there is a very high suction and it decreases downstream. With increasing α, the suction at the upstream corner further increases and the region extends, which is similar to a pressure distribution caused by conical vortices on a flat roof in oblique flow (Kawai and Nishimura 1996, Kawai 2002). Meanwhile, a remarkable higher-pressure region develops downstream. This type of pressure distribution, i.e., a low-pressure region followed by a relative high pressure, was termed a reattachment-type pressure distribution by Nakamura and Hirata (1994). This pressure distribution is the final stage of the shear-layer/edge interaction and plays a very important role in galloping (Nakamura *et al.* 1991, Nakamura and Hirata 1994).

In contrast to the forward inclination, increasing the backward inclination reduces the suction at the upstream corner of the free end; the pressure near the free end is substantially increased by the backward inclination, that is to say, the backward inclination produces a more positive pressure near the free end. The increase in the pressure is induced by a decrease in the curvature of the shear layer that is reported in Hu *et al.* (2015a). Meanwhile, Hu *et al.* (2015a) ascribed the decrease in the curvature to a suppression of the downwash near the free end by a severe upward

axial flow in the near wake of the backward inclined square prism. On the other hand, compared with the vertical case, a higher-suction region (C_p = -1) appears at the mid-span of the prism with a small backward inclination (i.e., α = -5°, -10° and -15°). The higher-suction region shrinks and finally disappears with increasing the backward inclination. Overall, the pressures on the side face increase with the backward inclination.

Mean pressure coefficients on the leeward face with different inclinations are presented in Fig. 7. For α = 0°, the pressure coefficient decreases from the bottom to the top and remains invariant in the mid-span region, which reflects a three-dimensionality in the wake of a cantilever prism and a near two-dimensionality at the mid-span. With increasing the forward inclination, the pressure coefficient generally increases over the leeward face except the region near the free end. In this region, the pressures significantly become smaller and the associated region shrinks as well. The significant smaller pressure near the free end could be attributed to the enhanced tip vortex pair in the near wake of forward inclined prism as reported by Hu *et al.* (2015c). However, for backward inclinations, the pressures near the free end increase with increasing the backward inclination, which induced by an absence of the tip vortex pair behind the free end of the backward inclined prism (Hu *et al.* 2015c). On the other hand, for small backward inclinations, pressures both in the free-end region and at the mid-span are lower than the surrounding pressures, and the smaller-pressure region shrinks with increase of the backward inclination. Furthermore, increasing the backward inclination from α = -5° to -35° generally increases the pressure on the whole face.

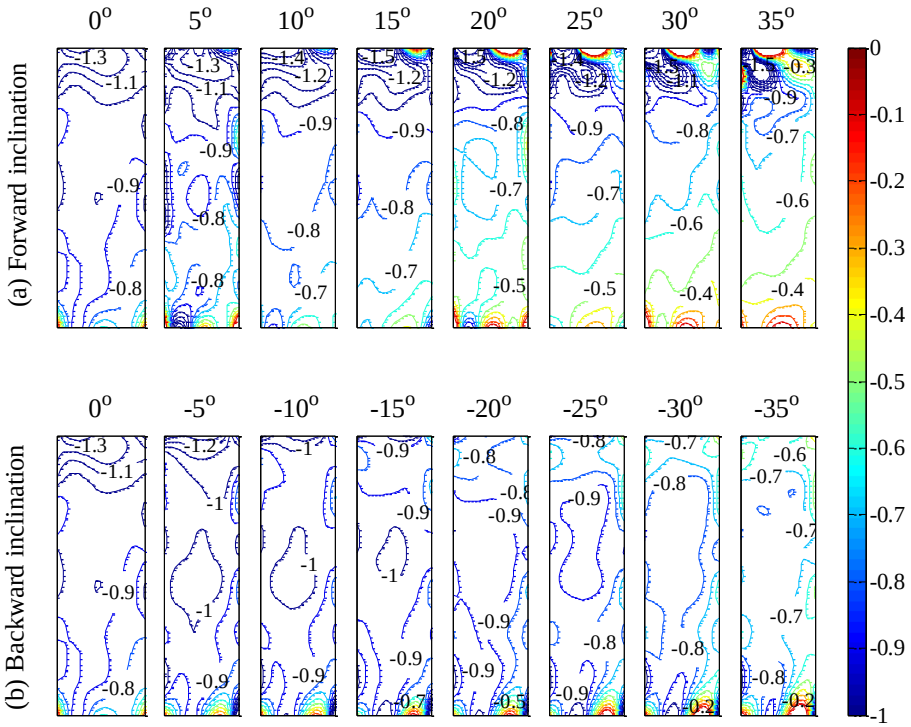

Fig. 6 Mean pressure coefficients on the side face with different inclinations

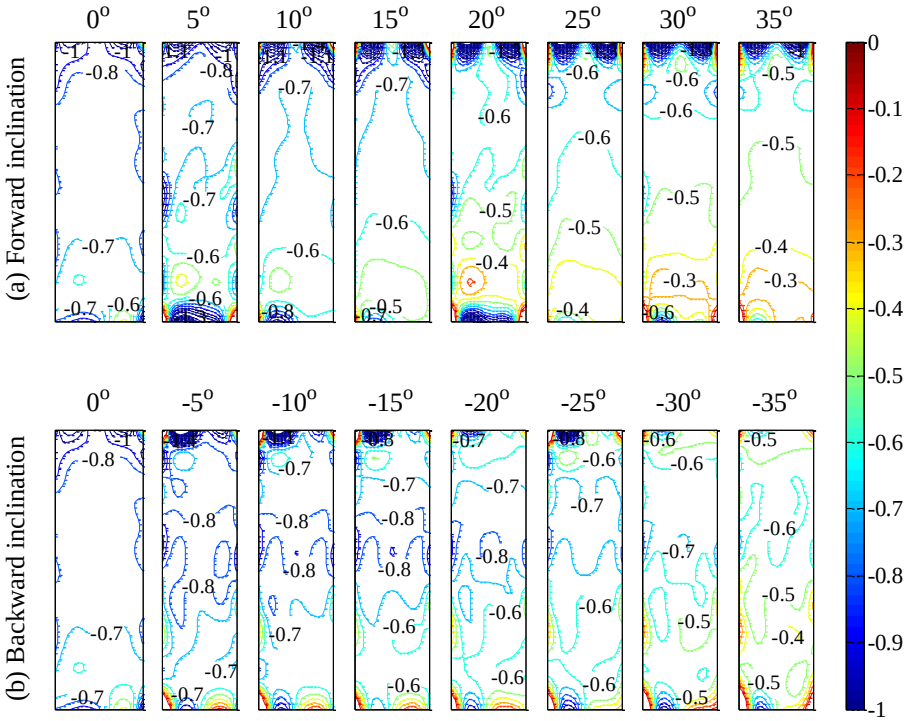

Fig. 7 Mean pressure coefficients on the leeward face of the prism with different inclinations

3.2 Force coefficients

3.2.1 Local force coefficients

For a three-dimensional prism with one end fixed on ground and another end set to be free, aerodynamic forces are varied throughout its span. The variation throughout the span is induced by the three-dimensional flow that consists of a downwash near the free end, a nearly two-dimensional flow at the mid-span and an upwash near the base (Wang and Zhou 2009, Hosseini *et al.* 2013, Sumner 2013). Furthermore, both forward and backward inclinations have a significant effect on the flow around the prism as reported by Hu *et al.* (2015c). As a result, local force coefficients are very likely changed by the inclinations. To evaluate the influence of the inclinations on local forces of the prism, the local force coefficients are shown in Figs. 8-10. The local force coefficients are defined as follow

$$C_D(z)=\frac{F_D(z)}{1/2\rho V_{ref}^2 Dh(z)}, C_D^{'}(z)=\frac{\sigma_D(z)}{1/2\rho V_{ref}^2 Dh(z)}, C_L^{'}(z)=\frac{\sigma_L(z)}{1/2\rho V_{ref}^2 Dh(z)}. \quad (1)$$

in which, $C_D(z)$, $C_D^{'}(z)$ and $C_L^{'}(z)$ are the local mean drag coefficient, the local RMS drag coefficient and the local RMS lift coefficient at elevation z, respectively; $F_D(z)$, $\sigma_D(z)$ and

$\sigma_L(z)$ are the local mean drag force, the local RMS drag force and the local RMS lift force.

The local mean drag coefficients of the prism with different inclinations are presented in Fig. 8. For the forward inclination cases, $C_D(z)$ over the entire span substantially decreases with increasing the forward inclination, which is a combined effect of a decrease in pressures on the windward face and a general increase on the leeward face with increasing forward inclination as shown in Figs. 5(a) and 7(a). Meanwhile, $C_D(z)$ increases progressively with height for all the cases. However, it suddenly increases near the free end for the cases with a large forward inclination angle (i.e., α = 25° and 35°), which is due to a high suction on the leeward face near the free end as presented in Fig. 7(a). For the backward inclination cases, $C_D(z)$ of the prism with a small inclination angle (i.e., α = -5°) is larger than that of the vertical prism over most of the span. As the backward inclination is increased to α = -15°, $C_D(z)$ is lower than that of the vertical prism. Further increasing the backward inclination decreases $C_D(z)$ significantly. However, the reduction in $C_D(z)$ caused by the backward inclination is not as large as that occurs in the forward inclination cases. In addition, a sudden increase near the free end gradually weakens with increasing the backward inclination and the increase becomes a decrease as α = -35°, which is caused by an increase in the pressures on the leeward face near the free end as shown in Fig. 7(b).

As shown in Fig. 9(a), increasing the forward inclination generally decreases the local RMS drag coefficient $C_D'(z)$ over the entire span of the prism, except an invariant in $C_D'(z)$ near the free end for $\alpha \leq 15°$. A dramatic increase in $C_D'(z)$ with height can be seen near the free end for large forward inclinations (i.e., $\alpha \geq 15°$), which might be due to the presence of an enhanced tip vortex pair (Hu *et al.* 2015c). Meanwhile, for these large inclinations, an obvious decrease with decreasing height is observed at the lower half span. For the backward inclination cases, $C_D'(z)$ for α = -5° and -15° is in general greater than that for α = 0°, apart from lower $C_D'(z)$ occurs near the free end for α = -15°. Beyond -15° (i.e., α = -25° and -35°), $C_D'(z)$ is lower than that for α = 0°, and $C_D'(z)$ decreases with increasing the backward inclination; a significant decrease with height is exhibited when *z/H* is approximately larger than 0.6, which may be because of the suppression of the tip vortex pair (Hu *et al.* 2015c).

The local RMS lift coefficient $C_L'(z)$ of the prism with different inclinations is shown in Fig. 10. It can be seen that increasing the forward inclination significantly decreases $C_L'(z)$ over the entire span of the prism except the free end region. For all the forward inclination cases and the vertical case, $C_L'(z)$ first increases with height and then decreases as *z/H* exceeds a critical value. The critical height decreases as the forward inclination is increased, and meanwhile the decrease in $C_L'(z)$ is less significant. $C_L'(z)$ of backward inclined prisms is shown in Fig. 10(b). For α = -5°, $C_L'(z)$ is remarkably larger than those for α = 0° over the entire span. Compared with α = -15°, $C_L'(z)$ for α = 0° is lower at certain heights (e.g., at the mid-span) but greater at other heights. The case with α = -25° in general has smaller $C_L'(z)$ along the height than the case with α = 0° apart from larger values near the mid-span. Further increasing the backward inclination angle to -35°

significantly decreases $C_L^{'}(z)$ to much lower values than those of the vertical case. A general overview of Fig. 10 suggests that the effect of the forward inclination on $C_L^{'}(z)$ is greater than that of the backward inclination.

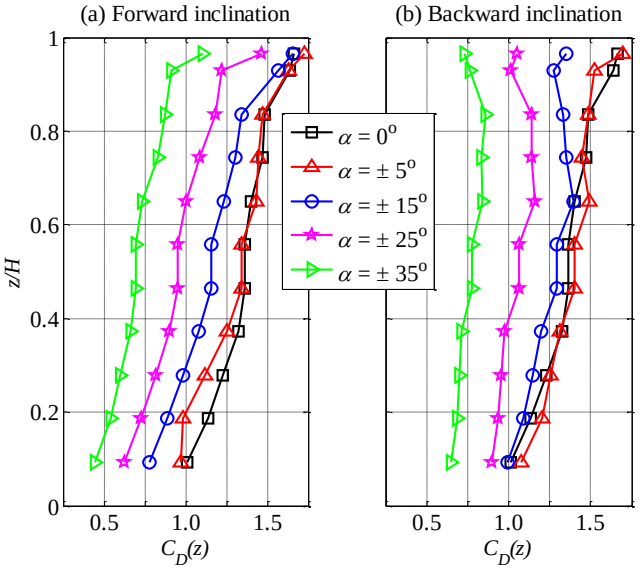

Fig. 8 Local mean drag coefficients of the prism with different inclinations

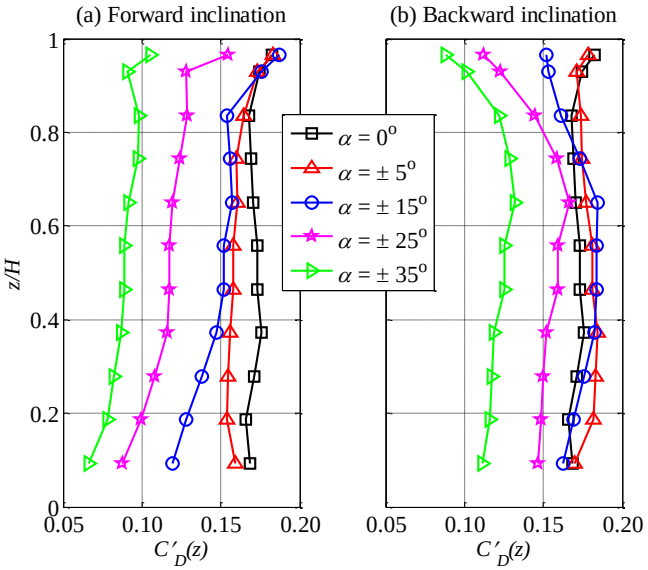

Fig. 9 Local RMS drag coefficients of the prism with different inclinations

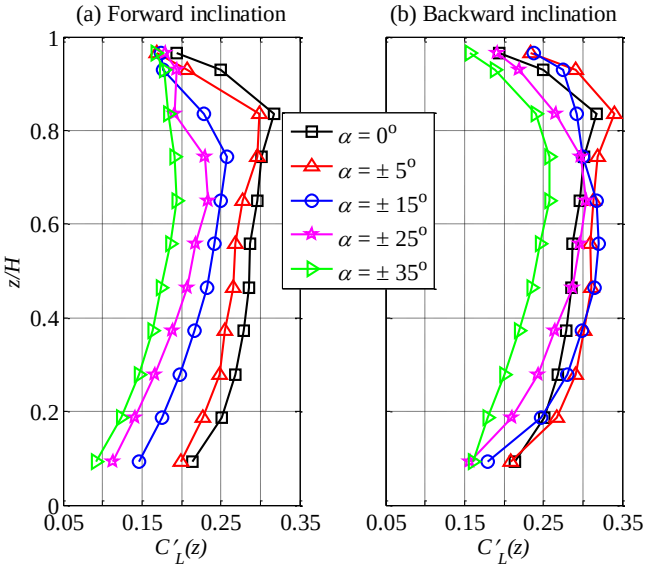

Fig. 10 Local RMS lift coefficients of the prism with different inclinations

3.2.2 Base force and moment coefficients

Base force and moment coefficients as a function of the inclination angle are presented in Figs. 11 and 12 respectively. The coefficients are defined as

$$C_D = \frac{F_D}{1/2\rho V_{ref}^2 DH}, C_D^{'} = \frac{\sigma_D}{1/2\rho V_{ref}^2 DH}, C_L^{'} = \frac{\sigma_L}{1/2\rho V_{ref}^2 DH},$$
$$C_{M_D} = \frac{M_D}{1/2\rho V_{ref}^2 DH^2}, C_{M_D}^{'} = \frac{\sigma_{M_D}}{1/2\rho V_{ref}^2 DH^2}, C_{M_L}^{'} = \frac{\sigma_{M_L}}{1/2\rho V_{ref}^2 DH^2}. \quad (2)$$

where C_D, $C_D^{'}$ and $C_L^{'}$ are the mean base drag, RMS base drag and RMS base lift coefficients respectively; C_{M_D}, $C_{M_D}^{'}$ and $C_{M_L}^{'}$ are the along-wind mean base moment coefficient, the along-wind RMS base moment coefficient and the across-wind RMS base moment coefficient respectively. F_D, σ_D and σ_L are the mean drag force, RMS drag force and RMS lift force at the model base; M_D, σ_{M_D} and σ_{M_L} are the corresponding base moments.

The mean base drag coefficient C_D, RMS base drag coefficient $C_D^{'}$ and RMS base lift coefficient $C_L^{'}$ of the prisms, including forward inclined ones, the vertical one and backward inclined ones, are presented in Fig. 11. The three coefficients of all backward inclined prisms are larger than values of the corresponding forward inclined prisms. In other words, the forward inclinations result in a more significant reduction on these coefficients than the backward inclinations. The observation is consistent with the phenomenon that the reduction in the local coefficients caused by the backward inclination is not as remarkable as that by the forward

inclination, as shown in Figs. 8-10. Furthermore, as shown in Fig. 11, these coefficients generally decrease with increasing the forward or backward inclination except a slight increase that occurs at small backward inclinations. That is to say, the maximum values of the coefficients occur at a small backward inclination rather than the vertical case; the maximum ones are exhibited at α = -5° for all the three coefficients. Additionally, for the fluctuating coefficients, i.e., $C_D^{'}$ and $C_L^{'}$, the coefficients at α = -10° are larger than the one corresponding to the vertical case as well. According to the above observations, the introduction of either forward or backward inclinations except small backward inclinations is beneficial to reduce wind-induced forces on structures and hence decrease the corresponding responses.

The base moment coefficients for both along-wind and across-wind directions are presented in Fig. 12. The along-wind mean base moment coefficient C_{M_D} generally decreases with increasing both the forward and backward inclination except for small backward inclinations, where C_{M_D} increases with the backward inclination.

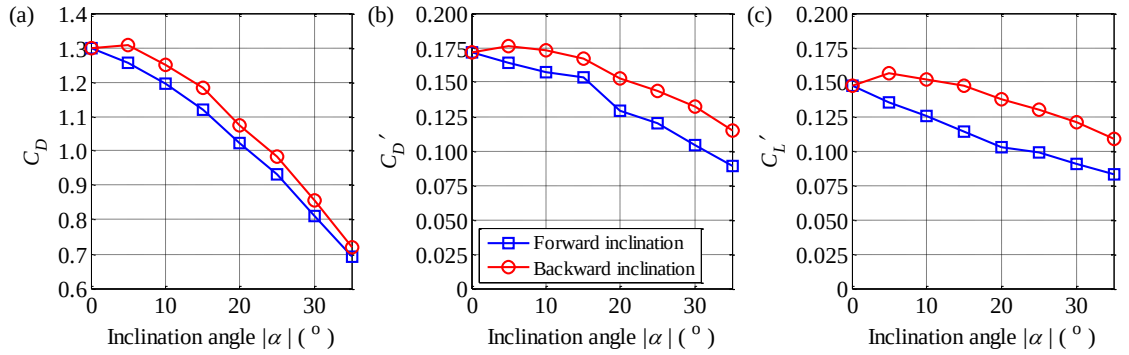

Fig. 11 Variation of force coefficients with inclination angle: (a) mean base drag coefficients, (b) RMS base drag coefficients and (c) RMS base lift coefficients

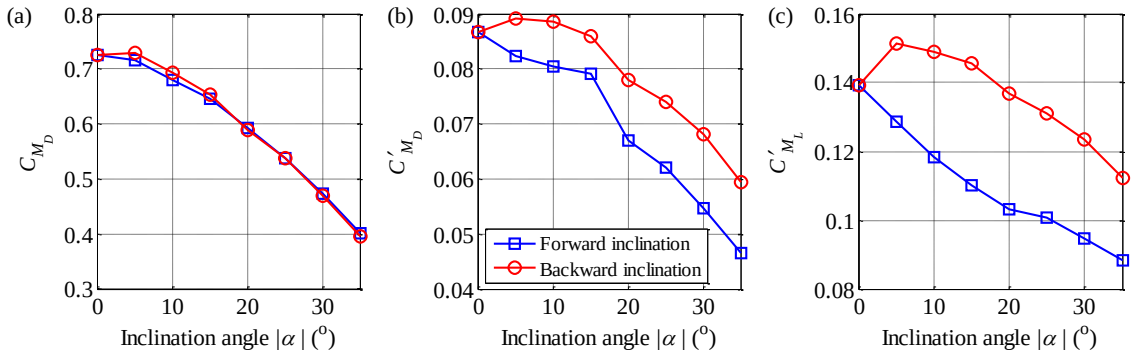

Fig. 12 Variations of base moment coefficients with inclination angle: (a) along-wind mean base moment coefficients, (b) along-wind RMS base moment coefficients and (c) across-wind RMS base moment coefficients

There is no significant difference observed in C_{M_D} between the forward and backward inclination cases, apart from slightly larger values for the backward inclination observed at small inclinations (from $|\alpha|$ = 0° to 15°). Both C'_{M_D} and C'_{M_L} decrease with increasing the forward inclination remarkably, while they first increase and then decrease with increasing the backward inclination. The maximum values of C'_{M_D} and C'_{M_L} for the backward inclination cases are exhibited at $|\alpha|$ = 5°.

3.3 Generalized force spectra

Spectra of generalized along-wind force for forward and backward inclined cylinders are given in Figs. 13 and 14, respectively. It can be seen that, for both the vertical case (α = 0°) and small inclination cases (i.e., α = 5° and -5°), a spectral peak is observed at a reduced frequency (fD/V_{ref}) of approximately 0.2. It is believed that the peak was induced by the Karman vortex shedding. Although the shedded vortices are typically considered to cause fluctuating forces transverse to the incident flow, the vortex-induced force, or even vibration, along the incident flow direction has also been observed and widely reported in the literature (Griffin and Ramberg 1976, Bearman 1984, Vandiver and Jong 1987, Williamson and Govardhan 2004, Bourguet *et al.* 2011). In addition, the vortex-induced vibration in the along-wind direction has already been proven to occur at a frequency approximately twice the Strouhal frequency. In the present study, both the vertical case and small inclination cases exhibit the peak at $fD/V_{ref} \approx 0.2$, i.e., twice the Strouhal frequency, which by and large verifies that the peaks are likely induced by Karman vortex shedding. For larger inclinations, the peak is absent, which indicates that the large inclination suppress the conventional Karman vortex shedding to some extent. In addition, as shown in Fig. 13, the energy is reduced slightly with increasing the forward inclination. In contrast, differences between the spectra of backward inclinations are in general negligible, as shown in Fig. 14. These observations are generally consistent with the energy associated with along-wind force which is dominated by the oncoming flow condition as reported by Holmes (2015).

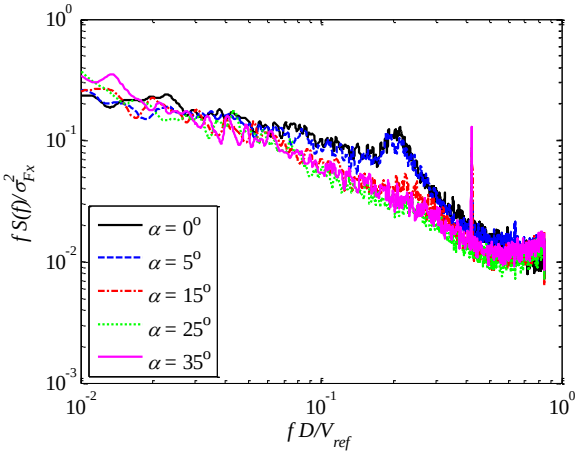

Fig. 13 Spectra of generalized along-wind force for forward inclined cylinders

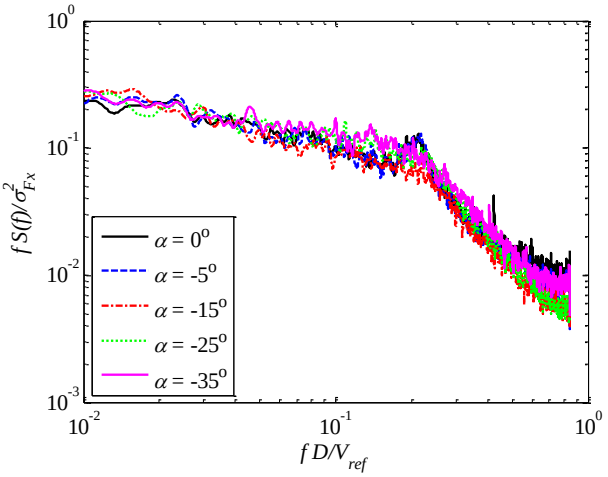

Fig. 14 Spectra of generalized along-wind force for backward inclined cylinders

For the generalized crosswind force spectra, the forward inclinations have noticeable effects. The energy is reduced significantly with increasing the forward inclination as shown in Fig. 15. Meanwhile, the spectral peak is weakened and the corresponding frequency shifts to the lower end as well. Since the crosswind force spectral peak is primarily resulted from the vortex shedding on the two sides, it is believed that the forward inclination disrupts the vortex shedding and hence reduces the associated energy adjacent to the Strouhal frequency. For the backward inclination cases, as shown in Fig. 16, the change in the spectral energy distribution due to inclination is not as significant as that observed in the forward inclination cases. A slight increase in the spectral peak is observed at α = -5° compared with the vertical case. Whilst large backward inclinations (i.e., α = -15°, -25°, and -35°) gradually decrease the peak amplitudes.

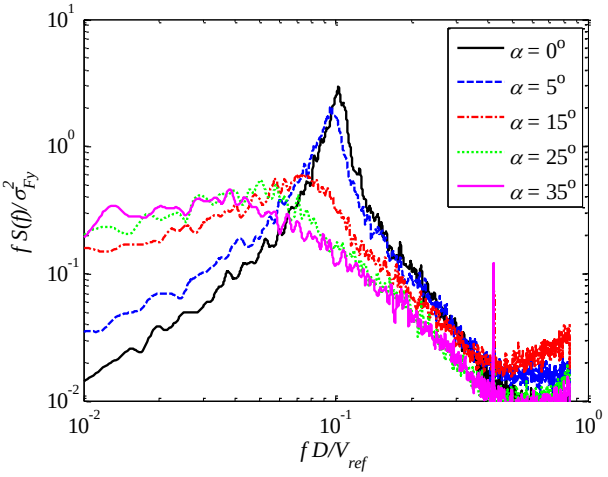

Fig. 15 Spectra of generalized crosswind force for forward inclined cylinders

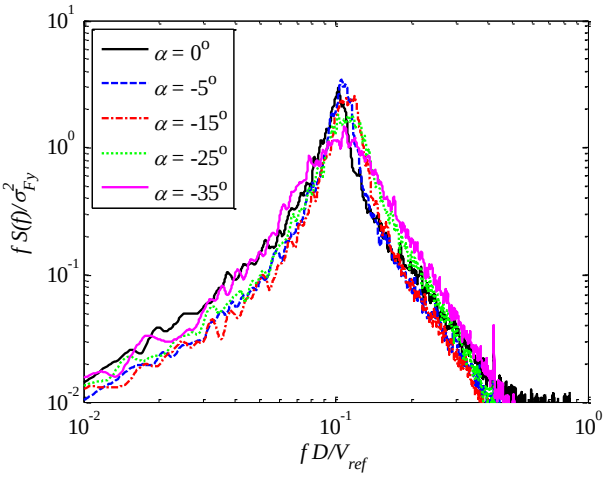

Fig. 16 Spectra of generalized crosswind force for backward inclined cylinders

3.4 Spectral analyses of pointwise pressures

Spectra of surface pressures at the points distributed along three vertical lines (Columns A, C, and E) and three levels (Levels 1, 6, and 10) on the side face (as shown in Fig. 17) of the prism with different inclinations are presented in Figs. 18 and 19. The spectral analyses are capable of evaluating local vortex shedding characteristics and separated shear layer behaviors.

For the vertical case (α = 0°), a well-defined peak is exhibited at a reduced frequency of approximately 0.1 in each spectrum as shown in Fig. 18. The energy peaks correspond to fluctuations induced by the Karman vortex shedding, and the corresponding frequency is referred to as the Strouhal frequency. A significant reduction in the energy peak at the Strouhal frequency toward the trailing edge (from Column A to E) and a resultant increase in the energy in the higher-frequency range are observed at all three levels. The phenomenon that the energy transfers to the higher-frequency range from the leading edge to the trailing edge agrees with those reported in the literature (Kareem and Cermak 1984, Surry and Djakovich 1995). These studies attributed the transfer in the energy to a possible intermittent reattachment of separated shear layers on the side face near the trailing edge. In addition, compared with Level 1, less significant reductions in the energy peak from Column A to E are observed at the other two lower levels (i.e., Levels 6 and 10). Meanwhile, the energy peaks at the two levels at the three columns have appreciably larger amplitudes than those at Level 1; the peaks at Level 6 have the largest amplitude. These observations indicate that both the free-end flow and the base flow have to some extent disrupted the vortex shedding in the corresponding regions whilst have less influence on the flow field at the mid-span (i.e., Level 6). The downwash flow near the free end and the upwash flow near the base for a square prism have been widely reported in the literature (Saha 2013, Uffinger *et al.* 2013, Wang *et al.* 2013, Hu *et al.* 2014, Hu *et al.* 2015c).

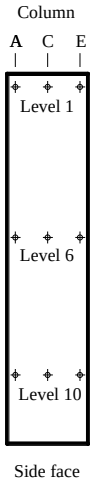

Fig. 17 Pressure taps selected to perform spectral analyses on their pressures in Figs. 18 and 19

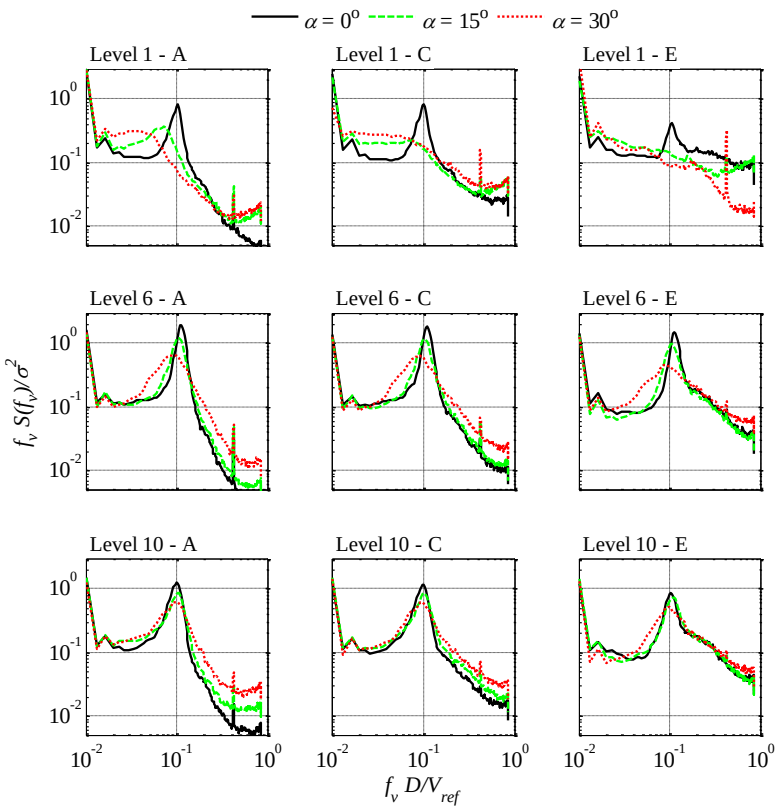

Fig. 18 Spectral analyses of pressure coefficients on the side face at three columns (Columns A, C, E) and three levels (Levels 1, 6, 10) of forward inclined prisms (α = 15° and 30°) and vertical prism (α = 0°)

A general overview of Fig. 18 suggests that the effect of the forward inclination on the energy distribution becomes less pronounced from Level 1 to Level 10 (i.e., from the free end to the base). At Level 1, increasing the forward inclination considerably reduces the amplitude of the peak and the reduction becomes more remarkable from Column A to E (i.e., from the leading edge to the trailing edge). Furthermore, at Column A, the peak shifts toward the lower-frequency region with increasing the forward inclination, indicating that the energy associated with vortex shedding is shifted toward the lower-frequency range. Meanwhile, the peak around the Strouhal frequency is generally absent at Columns C and E. The appreciable suppressions of the peak at Level 1 in the forward inclination cases can be explained by a significant increase in the curvature of the separated shear layer near the free end, which is reported in the study of Hu *et al.* (2015a). The significant increase in the curvature results in considerable interactions between the shear layer and the side face. Consequently, the vortex shedding process is suppressed. At Level 6, with increasing the forward inclination, the amplitude of the peak is reduced to some extent and the peak shifts toward the lower-frequency region as well; both trends are less significant than those observed at Level 1. At Level 10, the influences of the forward inclination on the peak amplitude and the associated frequency are very limited.

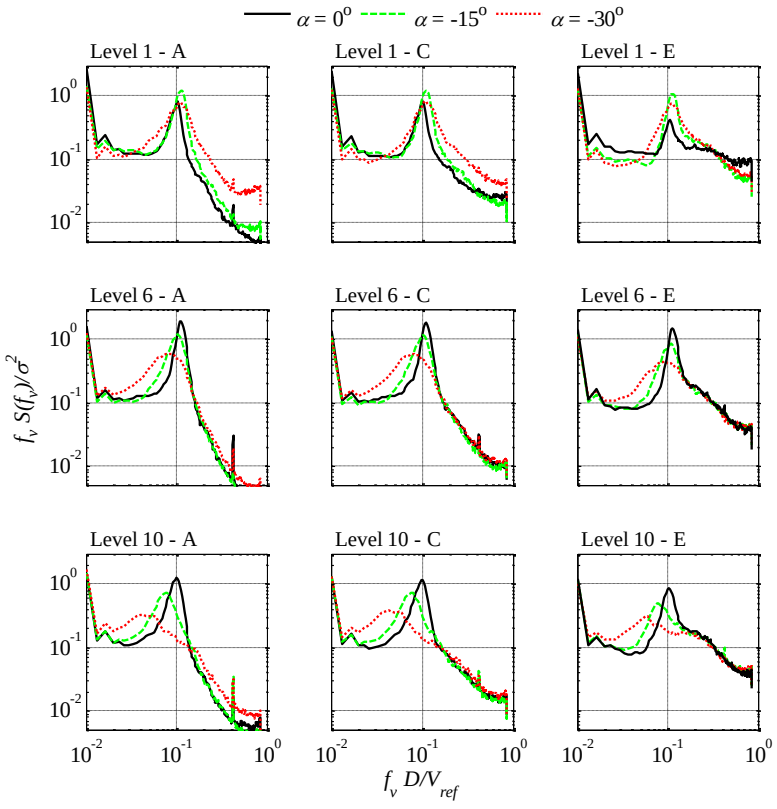

Fig. 19 Spectral analyses of pressure coefficients on the side face at three columns (Columns A, C, E) and three levels (Levels 1, 6, 10) of backward inclined prisms (α = -15° and -30°) and vertical prism (α = 0°)

Spectral analyses of the pointwise pressures on the side face of backward inclined prisms compared with the vertical case are presented in Fig. 19. At Level 1, the energy peaks for all backward inclination cases are more pronounced than the peak of the vertical case at the three columns, which is opposite to the effect of the forward inclination on the spectra at Level 1. Meanwhile, the peak for α = -15° is more sharp than that for α = -30°. Furthermore, from Column A to E, the amplitudes of the peaks generally remain invariant for the two backward inclination cases, unlike the vertical case where the peak amplitude decreases from Column A to E. The presence of sharper peaks in the spectra for the backward inclination cases can be attributed to a smaller curvature of the shear layer at Level 1 for the backward inclination cases compared with the vertical case as reported by Hu *et al.* (2015a). The smaller the curvature of the shear layer is, the lower probability the interaction between the shear layer and the trailing edge has. As a result, the vortex shedding keeps regular and induces the same effect along the streamwise direction (i.e., from Column A to E) at Level 1. Contrary to Level 1, at Levels 6 and 10, increasing the backward inclination decreases the amplitude of the energy peak and shifts the peak toward the lower-frequency region, similar to the trend caused by the forward inclination. However, the backward inclination results in a more notable influence at Level 10 than at Level 6, which is opposite to the observation in the forward inclination cases. The significant influence near the base of the backward inclined prism is caused by a significant increase in the curvature of the shear layer as suggested by Hu *et al.* (2015a).

3.5 Coherences of pressures on two side faces

Coherences between surface pressures taken at the corresponding positions on two side faces are shown in Figs. 20 and 21 Pressures at three levels (i.e., Levels 1, 6, and 10) and three columns (i.e., Columns A, C, and E) are evaluated. The coherence is defined by the following equation

$$coh_{p_r p_l} = \frac{\left|S_{p_r p_l}\right|}{\sqrt{S_{p_r p_r}}\sqrt{S_{p_l p_l}}} \tag{3}$$

where $coh_{p_r p_l}$ is the coherence between the pressure on the right side face (p_r) and the pressure on the left side face (p_l); $S_{p_r p_l}$ is the cross-power spectrum between p_r and p_l; $S_{p_r p_r}$ and $S_{p_l p_l}$ are the auto-power spectrum of p_r and p_l respectively.

Coherences of pressures on two side faces of forward inclined prisms (i.e. α = 15° and 30°) and vertical prism (i.e., α = 0°) are shown in Fig. 20. For the vertical prism, high coherences are exhibited at the Strouhal frequency for all the evaluated levels and columns. Overall, the coherence at the mid-level, i.e., Level 6, is higher than that at the level near the free end (Level 1) and the base (Level 10); the coherence at the mid-column, i.e. Column C, is higher than that at other two columns, one near the leading edge (Column A) and another one near the trailing edge (Column E).

For the forward inclination cases, coherences at the Strouhal frequency are considerably reduced at Level 1. The reductions of the coherences are induced by the presence of a significant downward axial flow in the near wake of forward inclined prism near the free end (Hu and Tse 2014, Tse *et al.* 2014, Hu *et al.* 2015c), which interrupts the communication or interaction of the shear layer at two sides (Matsumoto *et al.* 2010). As height decreases, the coherence around the Strouhal frequency progressively recovers to a high level but still lower than that of the vertical

case. It is noted that significant peaks are observed at around four times the Strouhal frequency. The origination of such a high frequency component in the fluctuating pressure may result from acoustic signals.

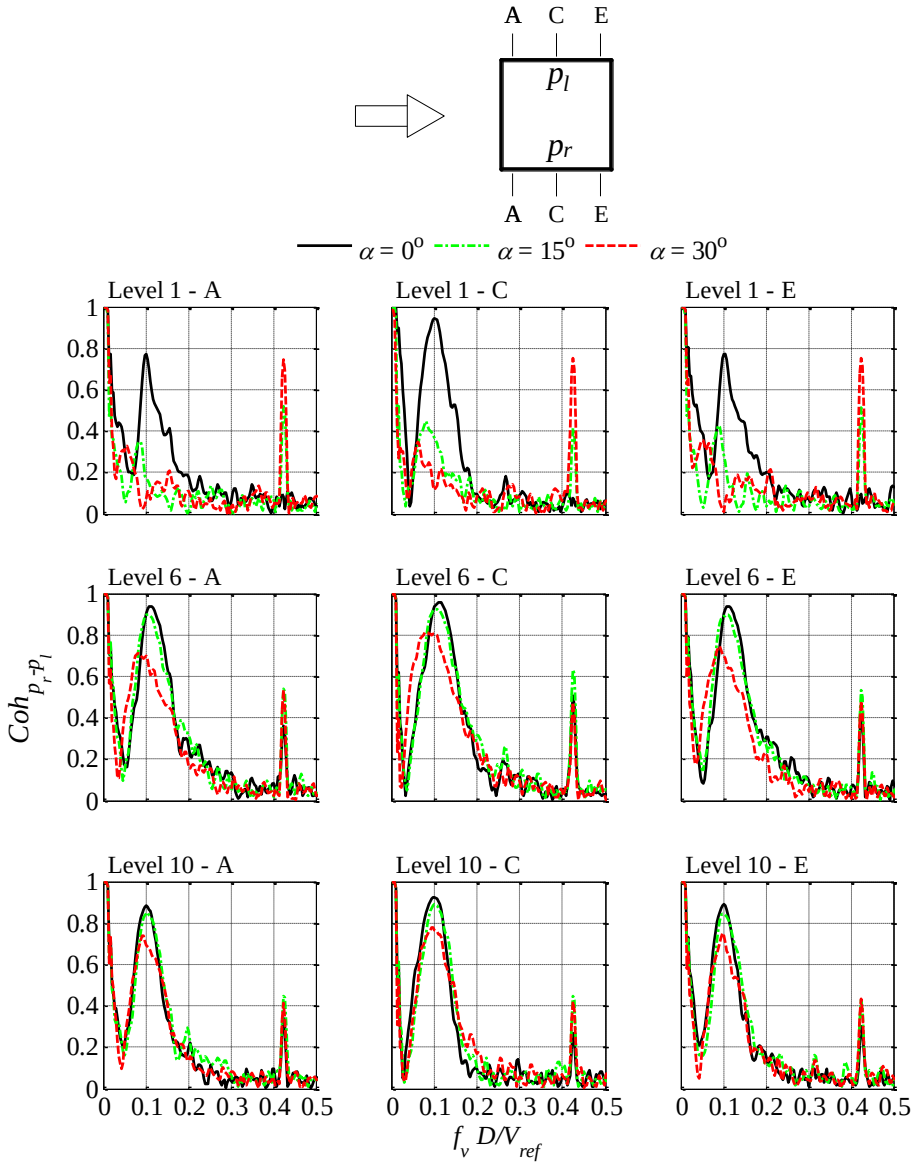

Fig. 20 Coherences between surface pressures taken at the corresponding positions on two side faces of forward inclined prisms compared with vertical prism

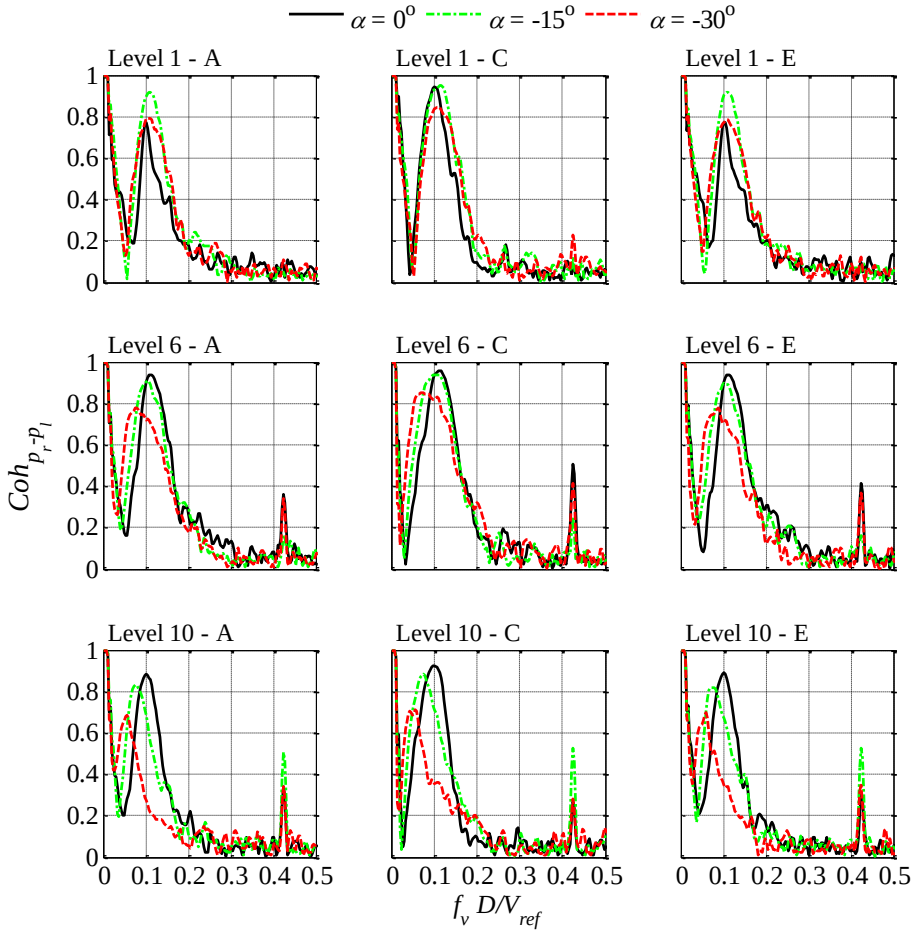

Fig. 21 Coherences between surface pressures taken at the corresponding positions on two side faces of backward inclined prisms compared with vertical prism

For the backward inclination cases, variations in the coherence at the top level (Level 1) are quite different from those observed in the forward inclination case. At Columns A and E, coherences at the Strouhal frequency for backward inclination cases (α = -15° and -30°), particularly for α = -15°, are higher than those for the vertical case. At Column C, the coherence for α = -15° is comparable to that for α = 0°, and the coherence for α = -30° is slightly lower than that for α = 0°. All these observations are generally consistent with the results shown in the above spectral analyses. On the other hand, with decreasing height, from Level 1 to Level 10, coherences around the Strouhal frequency for the backward inclination cases reduce. Meanwhile, the frequency corresponding to the coherence peak decreases with increasing the backward inclination. Compared with the reductions in coherences at the top level of forward inclined prisms, decreases near the base of backward inclined prism are much less significant. The less significant decreases are ascribed to an upward axial flow in the near wake of backward inclined prism and furthermore the upward axial flow is less intense than the downward axial flow behind the free end of forward

inclined prism (Hu and Tse 2014, Hu *et al.* 2014, Tse *et al.* 2014). Likewise, high coherences are exhibited at approximately four times the Strouhal frequency at Levels 6 and 10. Moreover, the coherences at Level 10 are higher than those at Level 6, and these coherence peaks are absent at Level 1. This trend is opposite to that in the forward inclination cases, in which the coherences at four times the Strouhal frequency increase with height. The fluctuating component with such a high frequency in the pressure needs further studies to reveal.

3.6 Strouhal numbers

The global Strouhal numbers (*St*), which are the mean value of the local Strouhal numbers over the whole span, of the prism with different inclinations are presented in Fig. 22. For the forward inclination, the variation in *St* with the inclination angle is straightforward. Increasing the forward inclination weakens the vortex shedding significantly and decreases *St* monotonously. A forward inclination angle of 35° results in a decrease of approximately 23% in *St*. Based on local Strouhal numbers reported by Hu *et al.* (2015b), it can be inferred that the reduction in *St* by the forward inclination is attributed to decreases in the local *St* in the upper part of the prism. Furthermore, Hu *et al.* (2015c) have ascribed the reduction in local *St* in the upper part to a downward axial flow generated by the forward inclination as mentioned before.

The variation in *St* caused by backward inclinations is different from that induced by forward inclinations. With increasing the backward inclination, *St* first increases until $|\alpha| = 10°$. Beyond 10°, the Strouhal number reduces monotonously. For 15°, it has a comparable *St* to that of the vertical case. The reductions in *St* for the large backward inclinations (>15°) are mainly due to reductions in local *St* in the lower part of the prism, which is described in Hu *et al.* (2015b). Because the backward inclination results in an upward axial flow in the near wake of the prism; the axial flow interacts with the Karman vortex and hence delays its shedding (Hu *et al.* 2015c). The increases in *St* for the small backward inclinations (5° and 10°) are largely attributed to increases in local *St* near the free end, which is induced by the suppression of the downwash. The suppression is caused by the upward axial flow as shown in numerical results in Hu *et al.* (2014) and (Hu *et al.* (2015c)). In addition, the Strouhal number for the backward inclination case is larger than that of the corresponding forward inclination case.

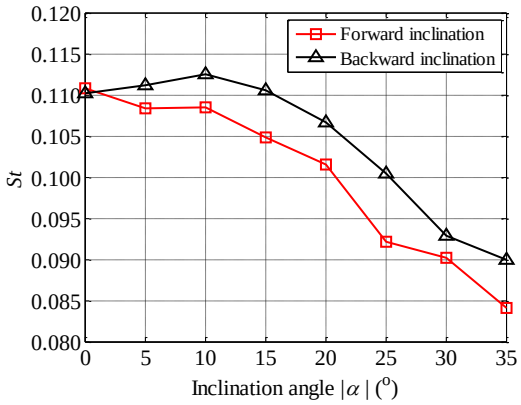

Fig. 22 Global Strouhal numbers of the prism with different inclinations

4. Conclusions

This study investigated influences of inclinations on aerodynamic characteristics of a square-section prism. Pressures acting on a static square prism with different inclinations were measured in a wind tunnel. The tested inclinations included forward inclinations (inclined to the upwind direction), a vertical attitude, and backward inclinations (inclined to the downwind direction).

The results show that both forward and backward inclinations have significant influences on aerodynamic characteristics, e.g., force coefficients, pressure distributions on the surface, vortex shedding of a square prism. Furthermore, the influences of forward and backward inclinations on these aerodynamic characteristics are quite different. The influences on the aerodynamic characteristics are explained by observations in previous studies. The major findings are briefly listed as follows:

(1) Mean pressure coefficients on the windward face substantially decrease with both forward and backward inclinations. The forward inclination moves the stagnation region upward whereas the backward inclination moves the region downward. That is to say, the stagnation region moves toward the upstream end of the inclined prism.
(2) Forward inclinations result in a reattachment-type pressure distribution near the free end on the side face. This pressure distribution plays a very important role in galloping. Overall, the pressures on the side face increase with the backward inclination.
(3) Mean pressures over the leeward face except the region near the free end are increased by increasing the forward inclination. In the region near the free end, the pressures become smaller significantly. The significant smaller pressure near the free end could be attributed to the enhanced tip vortex pair in the near wake of forward inclined prism. However, the pressures near the free end increase with increasing the backward inclination, which induced by an absence of the tip vortex pair behind the free end of the backward inclined prism.
(4) Base forces and moments are in general reduced by both forward and backward inclinations, apart from an increase induced by small backward inclinations.
(5) Forward inclinations significantly suppress vortex shedding near the free end of the prism whereas backward inclinations suppress them near the base. The two types of inclination result in the effects on coherences between surface pressures taken at the corresponding positions on two side faces similar to their effects on vortex shedding.
(6) Similar to the variation trend in forces and moments with the inclinations, the Strouhal number is also reduced by both forward and backward inclinations, apart from larger Strouhal numbers observed in the small backward inclination range ($\alpha < 15°$) than that for the vertical case.

Acknowledgments

The authors appreciate technical assistances for the wind tunnel test provided by the staff in the CLP Power Wind/Wave Tunnel Facility at The Hong Kong University of Science and Technology.

References

Bearman, P.W. (1984), "Vortex shedding from oscillating bluff bodies", *Annu. Rev. Fluid Mech.*, **16**(1), 195-222.

Bourguet, R., Karniadakis, G.E. and Triantafyllou, M.S. (2011), "Vortex-induced vibrations of a long flexible cylinder in shear flow", *J. Fluid Mech.*, **677**, 342-382.

Griffin, O.M. and Ramberg, S.E. (1976), "Vortex shedding from a cylinder vibrating in line with an incident uniform flow", *J. Fluid Mech.*, **75**(2), 257-271.

Holmes, J.D. (2015), *Wind Loading of Structures*, CRC Press

Hosseini, Z., Bourgeois, J.A. and Martinuzzi, R.J. (2013), "Large-scale structures in dipole and quadrupole wakes of a wall-mounted finite rectangular cylinder", *Exp. Fluids*. **54**(9), 1-16.

Hu, G. and Tse, K.T. (2014). "The effect of inclination on galloping of square cylinder and its mechanism", *Proceedings of the 27th KKHTCNN Symposium on Civil Engineering*, Shanghai, China, November.

Hu, G., Tse, K.T. and Kwok, K.C.S. (2014), "Numerical investigation of aerodynamic characteristics of inclined finite square cylinders", *Proceedings of the Annual Conference of the Institute for Infrastructure Engineering*, Sydney, Australia, December.

Hu, G., Tse, K.T. and Kwok, K.C.S. (2015a), "Aerodynamic mechanisms of galloping of an inclined square cylinder", *J. Wind Eng. Ind. Aerod*., Under review.

Hu, G., Tse, K.T. and Kwok, K.C.S. (2015b), "Galloping of forward and backward inclined slender square cylinders", *J. Wind Eng. Ind. Aerod.*, **142**, 232-245.

Hu, G., Tse, K.T., Kwok, K.C.S. and Zhang, Y. (2015c), "Large eddy simulation of flow around inclined finite square cylinders", *J. Wind Eng. Ind. Aerod*., **146**, 172-184.

Kareem, A. (1990), "Measurements of pressure and force fields on building models in simulated atmospheric flows", *J. Wind Eng. Ind. Aerod.*, **36**, 589-599.

Kareem, A. and Cermak, J.E. (1984), "Pressure fluctuations on a square building model in boundary-layer flows", *J. Wind Eng. Ind. Aerod*., **16**(1), 17-41.

Kawai, H. (2002), "Local peak pressure and conical vortex on building", *J. Wind Eng. Ind. Aerod.*, **90**(4-5), 251-263.

Kawai, H. and Nishimura, G. (1996), "Characteristics of fluctuating suction and conical vortices on a flat roof in oblique flow", *J. Wind Eng. Ind. Aerod*., **60**, 211-225.

Kwok, K.C.S. and Melbourne, W.H. (1981), "Wind-induced lock-in excitation of tall structures", *J. Struct. Division*, **107**(1), 57-72.

Lin, N., Letchford, C., Tamura, Y., Liang, B. and Nakamura, O. (2005), "Characteristics of wind forces acting on tall buildings", *J. Wind Eng. Ind. Aerod*., **93**(3), 217-242.

Matsumoto, M., Yagi, T., Hatsuda, H., Shima, T., Tanaka, M. and Naito, H. (2010), "Dry galloping characteristics and its mechanism of inclined/yawed cables", *J. Wind Eng. Ind. Aerod*., **98**(6-7), 317-327.

Nakamura, Y. and Hirata, K. (1994), "The aerodynamic mechanism of galloping", *T JPN Soc. Aeronaut. S.* **36**(114), 257-269.

Nakamura, Y., Hirata, K. and Urabe, T. (1991), "Galloping of rectangular cylinders in the presence of a splitter plate", *J. Fluids Struct.*, **5**(5), 521-549.

Saha, A.K. (2013), "Unsteady flow past a finite square cylinder mounted on a wall at low Reynolds number", *Comput. Fluids*., **88**, 599-615.

Standards Australia/Standards New Zealand (2002), *Structural Design-General Requirements and Design Actions, Wind Actions AS/NZS 1170.2*,

Sumner, D. (2013), "Flow above the free end of a surface-mounted finite-height circular cylinder: A review", *J. Fluids Struct.*, **43** 41-63.

Surry, D. and Djakovich, D. (1995), "Fluctuating pressures on models of tall buildings", *J. Wind Eng. Ind. Aerod.*, **58**(1-2), 81-112.

Tanaka, H., Tamura, Y., Ohtake, K., Nakai, M. and Chul Kim, Y. (2012), "Experimental investigation of aerodynamic forces and wind pressures acting on tall buildings with various unconventional

configurations", *J. Wind Eng. Ind. Aerodyn.*, **107-108**, 179-191.
Tse, K.T., Hu, G. and Kwok, K.C.S. (2014). "The effect of inclination on galloping of square cylinder and its mechanism", *Proceedings of the 7th International Symposium on Environmental Effects on Buildings and People: Actions, Influences, Interactions, Discomfort (EEBP VII)*, Cracow, Poland, October.
Uffinger, T., Ali, I. and Becker, S. (2013), "Experimental and numerical investigations of the flow around three different wall-mounted cylinder geometries of finite length", *J. Wind Eng. Ind. Aerod.*, **119**, 13-27.
Vandiver, J.K. and Jong, J.Y. (1987), "The relationship between in-line and cross-flow vortex-induced vibration of cylinders", *J. Fluids Struct.*, **1**(4), 381-399.
Wang, H.F. and Zhou, Y. (2009), "The finite-length square cylinder near wake", *J. Fluid Mech.*, **638**(1), 453-490.
Wang, Y.Q., Jackson, P.L. and Sui, J. (2013), "Simulation of turbulent flow around a surface-mounted finite square cylinder", *J. Thermophys. Heat Tr.*, **28**(1), 118-132.
Williamson, C.H.K. and Govardhan, R. (2004), "Vortex-induced vibrations", *Annu. Rev. Fluid Mech.*, **36** 413-455.

JH